Cyanide Binding to the Novel 4Fe Ferredoxin from *Pyrococcus furiosus*: Investigation by EPR and ENDOR Spectroscopy

Joshua Telser,[§,⊥] Eugene T. Smith,[‡] Michael W. W. Adams,*[,‡] Richard C. Conover,[†] Michael K. Johnson,*[,†] and Brian M. Hoffman*[,§]

Contribution from the Departments of Chemistry and Biochemistry and the Center for Metalloenzyme Studies, University of Georgia, Athens, Georgia 30602, and the Department of Chemistry, Northwestern University, Evanston, Illinois 60208

Received November 3, 1994[⊗]

Abstract: The hyperthermophilic archaeon *Pyrococcus furiosus* contains a 4-Fe ferredoxin (*Pf*-Fd) that differs from most other 4Fe-Fd's in that its $[Fe_4S_4]$ cluster is anchored to protein by only three cysteinyl residues. *Pf*-Fd also is of interest because in its reduced form, $[Fe_4S_4]^+$, the cluster exhibits both $S = {}^1/_2$ and $S = {}^3/_2$ spin states. Addition of excess cyanide ion converts the cluster exclusively to an $S = {}^1/_2$ state ($g_1 = 2.09$, $g_2 = 1.95$, $g_3 = 1.92$); however, dialysis restores the EPR signal of native reduced protein, indicating that the cluster is not irreversibly altered by cyanide. Both the native protein and protein in the presence of excess cyanide ion (*Pf*-Fd-CN) were investigated here using the techniques of electron paramagnetic resonance (EPR) and electron−nuclear double-resonance (ENDOR) spectroscopy. No evidence for a strongly coupled solvent-derived hydrogen (^1H or ^2H) from an OH^- or H_2O ligand in either spin state of the $[Fe_4S_4]^+$ cluster was observed, contrary to an earlier report. Rather, $^{1,2}H$ ENDOR characteristic of 4Fe-Fd's was seen for both native *Pf*-Fd and *Pf*-Fd-CN. *Pf*-Fd-CN was further investigated using $^{13}CN^-$ and $C^{15}N^-$ ligands. ^{13}C and ^{15}N ENDOR indicated that a single cyanide ion bound directly, with the cluster showing an unusually small contact interaction ($a_{iso}(^{13}C) \sim -3$ MHz, $a_{iso}(^{15}N) \sim 0$). This is in contrast to cyanide bound to monomeric low-spin Fe(III)-containing proteins such as transferrin and myoglobin, for which the ^{13}C hyperfine coupling has a large isotropic component ($a_{iso}(^{13}C) \approx -30$ MHz). The full ^{13}C and ^{15}N hyperfine tensors were determined by computer simulation of the ENDOR spectra. The $\boldsymbol{A}(^{13}C)$ is rotated by ~40° about g_2. The $\boldsymbol{g}$ and $\boldsymbol{A}(^{13}C)$ tensor information is combined with recently reported single-crystal EPR studies on $[Fe_4S_4]^{+,3+}$ model compounds and leads to a simple geometrical picture of cyanide binding to *Pf*-Fd, in which CN^- replaces the Asp-14 ligand and binds in an orientation similar to that of the Cys residue found in an ordinary 4Fe-4S ferredoxin. This reversible binding of an exogenous ligand may have implications for the catalytic activity of Fe-S enzymes.

Introduction

Iron−sulfur proteins are found in a wide variety of organisms and play diverse functional roles including electron transfer (as in the ferredoxins, Fd's) and chemical catalysis (as in the (de)-hydratase enzyme aconitase).[1−11] Other roles, including structural,[12] regulatory,[13,14] iron storage,[15] and generation/stabilization of radical intermediates,[16,17] have also been proposed.

Ferredoxins containing a cubane-type $[Fe_4S_4]^{n+}$ cluster bound to protein via four cysteinyl residues (4Fe-Fd's) comprise one of the most common types of electron transfer proteins. This type of $[Fe_4S_4]$ cluster may be transformed into one that can perform chemical catalysis by removal of one or more of the cysteinyl ligands and replacement by a more labile (exogenous or endogenous) ligand. The prototypical example is aconitase, a tricarboxylic acid cycle enzyme that catalyzes the conversion of citrate to isocitrate. Extensive studies of aconitase by Beinert and collaborators have shown that one of the Fe atoms of its single $[Fe_4S_4]$ cluster is not coordinated by cysteine but rather is bound by H_2O/OH^- in its resting state.[10,11,18,19] This absence of thiolate ligation allows the unique Fe site to bind and activate substrate during enzyme action. Numerous other hydrolase enzymes have also been shown to contain $[Fe_4S_4]$ clusters.[10,20−25]

Insight into the mechanism of catalysis by Fe-S enzymes can be obtained by generating a "model" Fe-S cluster for the

† Department of Chemistry and Center for Metalloenzyme Studies, University of Georgia.

‡ Department of Biochemistry and Center for Metalloenzyme Studies, University of Georgia.

§ Northwestern University.

⊥ Permanent address: Department of Chemistry, Roosevelt University, 430 S. Michigan Ave., Chicago, IL 60605.

* Address correspondence to this author at the Department of Chemistry, Northwestern University, Evanston, IL 60208-3113; Tel.: 708-491-3104; FAX: 708-491-7713; E-mail: bmh@nwu.edu.

⊗ Abstract published in *Advance ACS Abstracts*, April 15, 1995.

(1) Johnson, M. K. In *Encyclopedia of Inorganic Chemistry*; King, R. B., Ed.; Wiley: London, 1994; Vol. 4, pp 1896−1915.
(2) Cammack, R. *Adv. Inorg. Chem.* **1992**, *38*, 281−322.
(3) Lovenberg, W., Ed. *Iron−Sulfur Proteins*; Academic Press: New York, 1973−1977; Vol. I−III.
(4) Spiro, T. G., Ed. *Iron−Sulfur Proteins*; Wiley: New York, 1982.
(5) Que, L., Jr., Ed. *Metal Clusters in Proteins*; ACS Symposium Series 372; American Chemical Society: Washington, DC, 1988.
(6) Lindahl, P. A.; Kovacs, J. A. *J. Cluster Sci.* **1990**, *1*, 29−73.
(7) Ohnishi, T. *Curr. Top. Bioenerg.* **1987**, *15*, 37−65.
(8) Golbeck, J. H. *Biochim. Biophys. Acta* **1987**, *895*, 167−204.
(9) Beinert, H. *FASEB J.* **1990**, *4*, 2483−2491.
(10) Beinert, H.; Kennedy, M. C. *Eur. J. Biochem.* **1989**, *186*, 5−15.
(11) Kennedy, M. C.; Stout, C. D. *Adv. Inorg. Chem.* **1992**, *38*, 323−339.
(12) Kuo, C.-F.; McRee, D. E.; Fisher, C. L.; O'Handley, S. F.; Cunningham, R. P.; Rainer, J. A. *Science* **1992**, *258*, 434−440.
(13) Rouault, T. A.; Stout, D. C.; Kaptain, S.; Harford, J. B.; Klausner, R. D. *Cell* **1991**, *64*, 881−883.
(14) Switzer, R. L. *BioFactors* **1989**, *2*, 77−86.
(15) Thauer, R. K.; Schönheit, P. In *Iron−Sulfur Proteins*; Spiro, T. G., Ed.; Wiley: New York, 1982; pp 329−341.
(16) Frey, P. A.; Reed, G. H. *Adv. Enzymol.* **1993**, *66*, 1−39.
(17) Reichard, P. *J. Biol. Chem.* **1993**, *31*, 8383−8386.
(18) Werst, M. M.; Kennedy, M. C.; Beinert, H.; Hoffman, B. M. *Biochemistry* **1990**, *29*, 10526−10532.
(19) Robbins, A. H.; Stout, C. D. *Proteins: Struct., Funct., Genet.* **1989**, *5*, 289−312.
(20) Flint, D. H.; Emptage, M. H.; Finnegan, M. G.; Fu, W.; Johnson, M. K. *J. Biol. Chem.* **1993**, *268*, 14732−14742.
(21) Scopes, R. K.; Griffiths-Smith, K. *Anal. Biochem.* **1984**, *136*, 530−534.
(22) Dreyer, J.-L. *Eur. J. Biochem.* **1985**, *150*, 145−150.
(23) Kuchta, R. D.; Hanson, G. R.; Holmquist, B.; Abeles, R. H. *Biochemistry* **1986**, *25*, 7301−7307.
(24) Flint, D. H.; Emptage, M. H.; Guest, J. R. *Biochemistry* **1992**, *31*, 10331−10337.

0002-7863/95/1517-5133$09.00/0

application of metal and/or ligand substitution reactions. This model can be either totally synthetic[26-28] or a suitable Fe-S protein. Such a protein is the ferredoxin isolated from the hyperthermophilic archaeon *Pyrococcus furiosus*.[29-33] This is a small, monomeric protein (M_r 7000) containing a single $[Fe_4S_4]$ cluster bound by only three cysteinyl residues (Cys-11, Cys-17, Cys-56).[29-31] The fourth (Cys-14) is replaced by Asp, which furnishes a potential carboxylate ligand. Thus *P. furiosus* Fd (*Pf*-Fd) is a "model protein" in which exogenous ligand binding to an $[Fe_4S_4]$ cluster can be readily investigated. A recent communication has shown that cyanide ion binds to the $[Fe_4S_4]^+$ cluster in *Pf*-Fd and alters its EPR and MCD spectrum.[34] This paper extends that study through the use of 35 GHz electron paramagnetic resonance (EPR) and multinuclear ($^{1,2}H$, ^{13}C, ^{15}N) electron-nuclear double-resonance (ENDOR) spectroscopy on the reduced, $[Fe_4S_4]^+$ cluster of *Pf*-Fd both as the native protein and in the presence of excess cyanide. These techniques, which have been important in the study of a number of Fe-S proteins,[35-41] lead to a satisfying geometric model for the cyanide-bound cluster, while disclosing surprising features of the cyanide bonding.

Experimental Section

Protein Preparation. *P. furiosus* Fd was isolated under anaerobic conditions in the presence of 2 mM sodium dithionite as described previously.[29] Samples for spectroscopic studies were in 50 mM Tris/HCl buffer, pH 7.8, with 2 mM dithionite and were exchanged with the equivalent D_2O buffer by repeated concentration and dilution in an Amicon ultrafiltration cell. Sample concentrations were based on the molar absorption coefficient at 390 nm, ϵ_{390} = 17 000 M^{-1} cm^{-1}, for air-oxidized samples.[30] Samples for ENDOR were typically 1 mM in Fd, and cyanide-treated samples were incubated for 2 h with a 250-fold molar excess of a neutral solution of KCN.[34] Isotopically labeled KCN ($K^{13}CN$, 99% ^{13}C; $KC^{15}N$, 98% ^{15}N) was obtained from Cambridge Isotope Laboratories.

EPR and ENDOR Studies. X-band (~9.5 GHz) EPR spectra were recorded on a Bruker ER200D EPR spectrometer equipped with an Oxford Instruments ESR-9 flow cryostat. "Q"-band (actually K_a-band, 35 GHz) EPR and ENDOR spectra were recorded on a modified Varian E-109 spectrometer equipped with a liquid helium immersion dewar, described elsewhere.[38] All Q-band spectra were recorded at 2 K and in dispersion mode, under "rapid-passage" conditions.[36-38]

The single-crystal ENDOR transition frequencies for a nucleus, J, of spin $I = {}^1/_2$ (e.g., ^1H, ^{13}C, and ^{15}N) are given to first order by eq 1:[42]

$$\nu_\pm = |\nu_J \pm A^J/2| \quad (1)$$

where A^J is the orientation-dependent nuclear hyperfine coupling constant and ν_J is the nuclear Larmor frequency. If $\nu_J > A^J/2$, as is usually the case for protons in biological systems, then the ENDOR spectrum consists of a hyperfine-split doublet centered about the Larmor frequency. For $\nu_J < A^J/2$, as is the case for nuclei with small nuclear Larmor frequencies, the ENDOR spectrum consists of a Larmor-split doublet centered at $A^J/2$. For a nucleus with $I \geq 1$, quadrupole interactions also need to be considered. However, the quadrupolar nuclei encountered (^2H, ^{14}N, both $I = 1$) in this study are not analyzed at this level. Computer simulation and analysis of frozen-solution ENDOR spectra employed procedures and programs described elsewhere.[36-38,43,44]

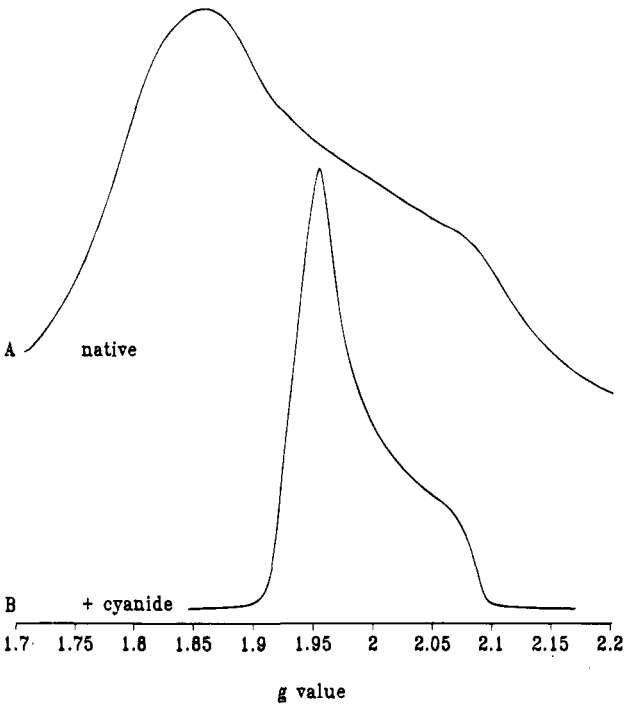

Figure 1. Dispersion-mode EPR spectra of *Pf*-Fd (A) as native protein and (B) in the presence of a 250 molar excess of KCN. Experimental conditions: (A) temperature, 2 K; microwave frequency, 35.13 GHz; microwave power, 1 mW; 100 kHz field modulation amplitude, 0.07 mT; time constant, 64 ms; (B) same as in (A) except, microwave frequency, 35.06 GHz; microwave power, 0.8 mW; time constant, 32 ms.

Results and Discussion

EPR of Reduced *Pf*-Fd and *Pf*-Fd-CN. The $[Fe_4S_4]^+$ cluster in *Pf*-Fd exists in two different spin states, $S = {}^1/_2$ and $S = {}^3/_2$.[30] This has been found for $[Fe_4S_4]^+$ clusters in other proteins (e.g., *Azotobacter vinelandii* Fe protein[45]) and in $[Fe_4S_4(SR)_4]^{3-}$ model compounds.[28] The two spin states are in approximately a 1:4 ratio as previously determined by absorption-mode EPR at ~9.5 GHz and at multiple temperatures.[30] The EPR spectra reported here were measured in dispersion-mode at 35 GHz only at 2 K; Figure 1A shows a representative spectrum of the $S = {}^1/_2$ state, which appears as the absorption envelope rather than its derivative. The g values

(25) Flint, D. H.; Emptage, M. H. *J. Biol. Chem.* **1988**, *263*, 3558-3564.
(26) Holm, R. H.; Ciurli, S.; Weigel, J. A. *Prog. Inorg. Chem.* **1990**, *38*, 1-74.
(27) Holm, R. H. *Adv. Inorg. Chem.* **1992**, *38*, 1-71.
(28) Carney, M. J.; Papaefthymiou, G. C.; Spartalian, K.; Frankel, R. B.; Holm, R. H. *J. Am. Chem. Soc.* **1988**, *110*, 6084-6095.
(29) Aono, S.; Bryant, F. O.; Adams, M. W. W. *J. Bacteriol.* **1989**, *171*, 3433-3439.
(30) Conover, R. C.; Kowal, A. T.; Fu, W.; Park, Jae-B.; Aono, S.; Adams, M. W. W.; Johnson, M. K. *J. Biol. Chem.* **1990**, *265*, 8533-8541.
(31) Busse, S. C.; La Mar, G. N.; Yu, L. P.; Howard, J. B.; Smith, E. T.; Zhou, Z. H.; Adams, M. W. W. *Biochemistry* **1993**, *31*, 11952-11962.
(32) Adams, M. W. W. *Annu. Rev. Microbiol.* **1993**, *47*, 627-658.
(33) Adams, M. W. W. *Adv. Inorg. Chem.* **1992**, *38*, 341-396.
(34) Conover, R. C.; Park, J.-B.; Adams, M. W. W.; Johnson, M. K. *J. Am. Chem. Soc.* **1991**, *113*, 2799-2800.
(35) Moura, I.; Macedo, A.; Moura, J. J. G. In *Advanced EPR: Applications in Biology and Biochemistry*; Hoff, A. J., Ed.; Elsevier: Amsterdam, 1989; pp 813-838.
(36) Hoffman, B. M.; DeRose, V. J.; Doan, P. E.; Gurbiel, R. J.; Houseman, A. L. P.; Telser, J. In *EMR of Paramagnetic Molecules*; Biological Magnetic Resonance 13; Berliner, L. J., Reuben, J., Eds.; Plenum Press: New York, 1993; pp 151-218.
(37) Hoffman, B. M. *Acc. Chem. Res.* **1991**, *24*, 164-170.
(38) Hoffman, B. M.; Gurbiel, R. J.; Werst, M. M.; Sivaraja, M. In *Advanced EPR. Applications in Biology and Biochemistry*; Hoff, A. J., Ed.; Elsevier: Amsterdam, 1989; pp 541-591.
(39) Lowe, D. J. *Prog. Biophys. Mol. Biol.* **1992**, *57*, 1-22.
(40) Sands, R. H. In *Multiple Electron Resonance Spectroscopy*; Dorio, M. M., Freed, J. H., Eds.; Plenum Press: New York and London, 1979; pp 331-374.
(41) Orme-Johnson, W. H.; Sands, R. H. In *Iron-Sulfur Proteins*; Lovenberg, W., Ed.; Academic Press: New York, 1973; Vol. II, pp 195-238.
(42) Abragam, A.; Bleaney, B. *Electron Paramagnetic Resonance of Transition Ions*, 2nd ed.; Clarendon Press: Oxford, 1970.

Table 1. EPR Data for *P. furiosus* Fd and Other $S = {}^1/_2$ $[Fe_4S_4]^+$ Cluster-Containing Proteins and Model Compounds

	g_1	g_2	g_3	g_{av}
Pf-Fd	2.12	1.86	1.79	1.92
Pf-Fd-CN	2.09	1.95	1.92	1.99
aconitase (E)[a]	2.06	1.93	1.86	1.95
aconitase (ES)[b]	2.04	1.85	1.78	1.89
Bp-Fd[c]	2.06	1.92	1.88	1.95
*Av*2[d]	2.05	1.94	1.88	1.96
$[Fe_4S_4(SCH_2Ph)_4]^{3-}$ [e]	2.043	1.948	1.871	1.954
$[Fe_4S_4(SCH_2Ph)_4]^{3-}$ [f]	2.087	1.971	1.917	1.992
$[Fe_4S_4(SPh)_4]^{3-}$ [g]	2.090	1.968	1.877	1.978
$[Fe_4S_4]^+$ |1/2 2 4\)[h]				1.96

[a] Reference 18. E refers to resting-state reduced aconitase. [b] Reference 18. ES refers to reduced aconitase in the presence of substrate. [c] Reference 41. *Bp* refers to *Bacillus polymyxa*. [d] Reference 45. *Av*2 refers to *Azotobacter vinelandii* Fe protein (protein II). Data are for native protein. [e] Reference 63. Data from a single-crystal analysis for center I_R. [f] Reference 63. Data from a single-crystal analysis for center II_R. [g] Reference 66. Data from a single-crystal analysis for center A. [h] Reference 69. Theoretical calculation for this spin state.

determined for the $S = {}^1/_2$ state under these conditions (g = [2.12, 1.86, 1.79]; $g_{av} = 1.92$), in conjunction with computer simulations,[46] are in agreement with those previously reported at 9.5 GHz (g = [2.10, 1.87, 1.80]).[30] EPR parameters for *Pf*-Fd and relevant protein, synthetic, and theoretical $[Fe_4S_4]^+$ cluster systems are summarized in Table 1. Also notable is that under the conditions employed here, the $S = {}^3/_2$ state does not exhibit a feature at $g \approx 5.6$; only features at $g \approx 5.0$ and $g \approx 2.6$ are observed (data not shown). This is in agreement with the previous, variable-temperature (4−18 K) EPR measurements[30] in showing that the feature at $g \approx 5.6$ is due to the higher energy Kramers doublet of the $S = {}^3/_2$ system, and it confirms the reported zero-field splitting parameters of $D = 3.3\ cm^{-1}$ and $E = 0.73\ cm^{-1}$. Using these parameters, the Boltzmann populations of the two doublets at 2 K are in roughly a 150:1 ratio, making the $g \approx 5.6$ feature relatively unobservable. The third g value of the ground-state Kramers doublet should appear at $g \approx 1.7$. Unfortunately, this g value lies at the extreme edge of the 35 GHz EPR spectrometer's magnet (~1.45 T), precluding its confirmation.

The $[Fe_4S_4]^+$ cluster in *Pf*-Fd is dramatically altered by the addition of excess (~250-fold) cyanide ion, which converts the cluster quantitatively to an $S = {}^1/_2$ system. Variable-temperature MCD studies confirm an $S = {}^1/_2$ ground state for cyanide-treated *Pf*-Fd and show that cyanide perturbs both the ground and excited state electronic properties.[34] This effect was interpreted in terms of cyanide binding to the unique (non-cysteinyl coordinated) cluster Fe atom, as neither the 8Fe-Fd from *Clostridium pasteurianum* (which has complete Cys ligation) nor the $[Fe_3S_4]^+$ form of *Pf*-Fd shows any changes in the EPR spectrum upon addition of excess cyanide ion. In support of this interpretation, the effect of cyanide on the $[Fe_4S_4]^+$ form of *Pf*-Fd is reversible. Anaerobic gel filtration of the protein results in quantitative reversion to the native state, as evidenced by reappearance of the characteristic $S = {}^1/_2$, $S = {}^3/_2$ EPR signals.[34]

The EPR signal of cyanide-bound *Pf*-Fd, which quantitates to 1.0 spin/molecule, has much longer relaxation times than the native signal, as it is observable at temperatures up to 60 K in absorption mode.[34] The g values and relaxation properties of this Fe-S cluster are distinct from both the native protein in the $S = {}^1/_2$ state and other 4Fe ferredoxins as well (see Table 1). The 35 GHz dispersion-mode signal at 2 K is shown in Figure 1B and corresponds exactly to that reported in absorption mode at X-band and 20 K (g = [2.09, 1.95, 1.92]; $g_{av} = 1.99$). The spectrum shown in Figure 1B was recorded on protein in aqueous buffer. Addition of a glassing agent, such as ethylene glycol (30% v/v), led to even longer relaxation times as manifested by narrower EPR line width and saturation at minimum microwave power (~2 μW). As a consequence, ENDOR spectra were more readily obtained for protein in aqueous buffer absent glassing agent, and only such spectra are reported here.

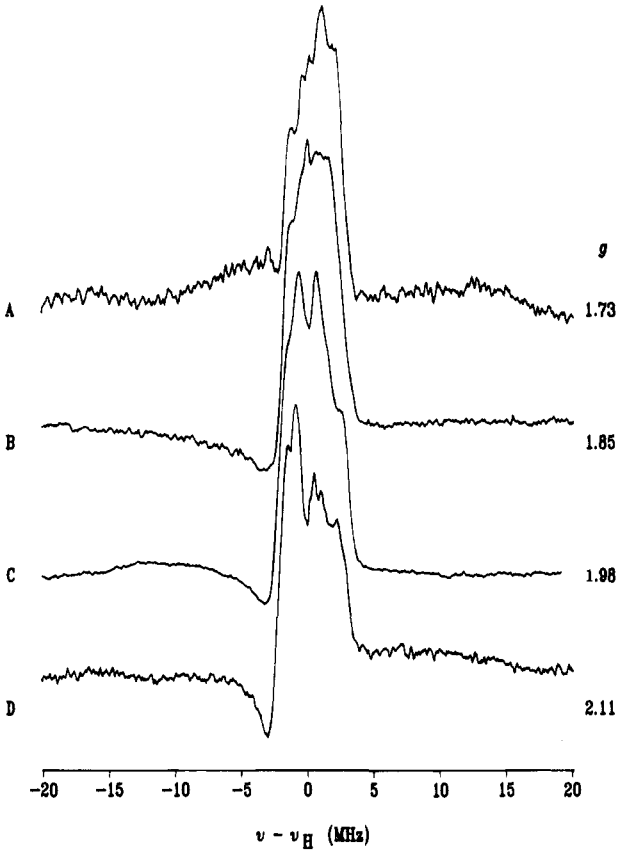

Figure 2. ^{1}H ENDOR spectra of native *Pf*-Fd in H_2O buffer (pH = 7.8). The spectra are centered at the proton Larmor frequency (ν_H = 50−60 MHz). Experimental conditions: (A) temperature, 2 K; microwave frequency, 35.04 GHz; microwave power, 0.2 mW; magnetic field, 1.445 T ($g = 1.73$); 100 kHz field modulation amplitude, 0.1 mT; time constant, 32 ms; rf scan rate, 2 MHz/s; rf power, 30 W; number of scans, 75; (B) same as in (A) except, magnetic field, 1.350 T ($g = 1.85$), 40 scans; (C) same as in (A) except, magnetic field, 1.265 T ($g = 1.98$), 50 scans; (D) same as in (A) except, magnetic field, 1.185 T ($g = 2.11$), 75 scans. No baseline correction was used.

^{1}H ENDOR of *Pf*-Fd and *Pf*-Fd-CN. Figure 2 presents 35 GHz ^{1}H ENDOR spectra of native *Pf*-Fd taken at magnetic field positions across the absorption envelope of the $S = {}^1/_2$ state. These ENDOR signals are due predominantly to the $S = {}^1/_2$ state, not $S = {}^3/_2$, because the signals dramatically diminish at a magnetic field position immediately below that corresponding to $g_1(\max) = 2.12$, where only the $S = {}^3/_2$ signal contributes. The pattern is centered at the proton Larmor frequency, ν_H = 50−60 MHz, as predicted by eq 1. The maximum breadth of the signal corresponds to the maximum proton hyperfine coupling, $A^H \sim 7-8$ MHz. This value is comparable to that seen for other $[Fe_4S_4]$ proteins, wherein A^H never has been found

(43) Hoffman, B. M.; Martinsen, J.; Venters, R. A. *J. Magn. Reson.* **1984**, *59*, 110−123.
(44) Hoffman, B. M.; Venters, R. A.; Martinsen, J. *J. Magn. Reson.* **1985**, *62*, 537−542.
(45) Lindahl, P. A.; Day, E. P.; Kent, T. A.; Orme-Johnson, W. H.; Münck, E. *J. Biol. Chem.* **1985**, *260*, 11160−11173.
(46) The program QPOW was used. See for example: Belford, R. L.; Belford, G. G. *J. Chem. Phys.* **1973**, *59*, 853−854.

to exceed 12 MHz.[18,36,47] The main qualitative point in these ^{1}H ENDOR spectra of $S = {}^1/_2$ native *Pf*-Fd is that there are no signals observed at $A^H > 10$ MHz (i.e., at more than 5 MHz removed from ν_H). This is in contrast to an earlier report from this laboratory,[48] in which a weak feature at ~69 MHz was observed near g_2(mid). This was assigned to ν_+ of a ^{1}H (or set of magnetically equivalent protons) with $A^H \approx 22$ MHz; no corresponding signal assignable to ν_- was seen. This signal was not observed for protein in D_2O solvent and was thus assigned to a water/hydroxide coordinated to the cluster's unique Fe atom. Corroboration was found in ^{2}H ENDOR spectra of protein in D_2O. Similar observations were reported for the $S = {}^3/_2$ form. However, since that early report, several independently prepared samples, using a variety of experimental conditions, have failed to reproduce this result (Figure 2 is representative of numerous such ^{1}H ENDOR spectra). We can only conclude that it was an artifact either of the sample or of the instrumentation: since the initial report, the isolation and purification of *Pf*-Fd have been optimized and considerable improvements have been made to the 35 GHz ENDOR spectrometer. Recent NMR evidence suggests that Asp-14 is instead coordinated to Fe,[49] as suggested by the primary sequence of *Pf*-Fd.

Higher resolution ^{1}H ENDOR spectra of native *Pf*-Fd in H_2O and D_2O show considerable structure that is associated with nonexchangeable protons (data not shown) from the β-CH_2 of cysteinyl ligands, as well as exchangeable resonances from weakly coupled protons, presumably associated with H-bonds to the cluster. ^{1}H ENDOR spectra of *Pf*-Fd-CN in H_2O and D_2O are analogous to those of the native protein: there are no signals corresponding to $A^H > 9$ MHz in either solvent, but there are numerous signals due to weakly coupled constitutive and solvent-exchangeable protons. Relaxation effects make it difficult to analyze quantitatively these ^{1}H ENDOR signals using CW ENDOR. Recently, the electron-spin-echo (ESE) ENDOR method has been used to characterize both the constitutive and solvent-exchangeable (H-bonded) protons in the $[Fe_3S_4]^+$ cluster of *Desulfovibrio gigas* hydrogenase.[50] We plan to apply this method to native and cyanide-bound *Pf*-Fd. The full analysis of the ^{1,2}H ENDOR spectra of *Pf*-Fd and *Pf*-Fd-CN using ESE-ENDOR is of interest not only in understanding the specific effect cyanide binding has on cluster conformation but also in understanding structural details of this extremely heat-stable protein.

^{13}C and ^{15}N ENDOR of *Pf*-Fd-CN. ENDOR studies using both $^{13}CN^-$ and $C^{15}N^-$ provide direct evidence for cyanide interaction with the $[Fe_4S_4]^+$ cluster of *Pf*-Fd. Figure 3 presents ENDOR spectra of *Pf*-Fd-CN with natural isotopic abundance cyanide ion (Figure 3C) and with the isotopologs $C^{15}N^-$ (Figure 3A) and $^{13}CN^-$ (Figure 3B), all taken at the minimum field of the EPR envelope, corresponding to $g_1 = 2.09$. The two spectra of isotopically enriched samples clearly display signals that are absent in the natural isotopic abundance sample. Neither of the isotopically enriched samples exhibited additional ENDOR signals at >20 MHz other than the characteristic ^{1}H feature centered at ν_H (55–60 MHz; *vide supra*). This is illustrated for the $^{13}CN^-$ sample in Figure 3D; its importance will be discussed below. As an additional check, samples for 35 GHz EPR/ENDOR were prepared containing the $[Fe_3S_4]^+$ form of

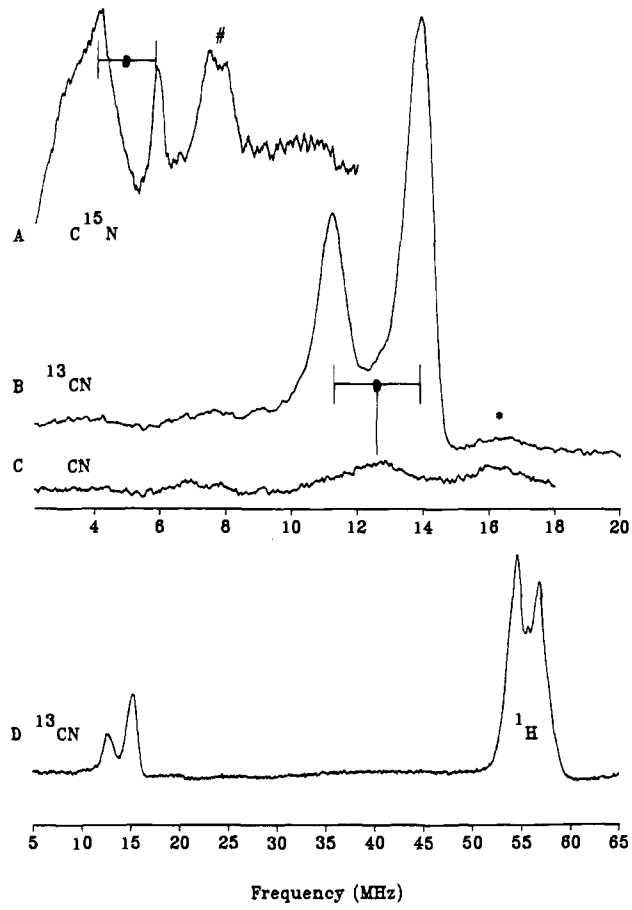

Figure 3. ENDOR spectra of (A) *Pf*-Fd-$C^{15}N$, (B,D) *Pf*-Fd-^{13}CN, and (C) *Pf*-Fd-CN. In (A) and (B), the ^{13}C and ^{15}N Larmor frequencies ($\nu_C = 12.7$ MHz; $\nu_N = 5.1$ MHz) are indicated by the crossbars indicate hyperfine coupling. The natural isotopic abundance ^{13}C feature is indicated in (C) by a connecting line to the corresponding point in (B). An additional weak feature in both (B) and (C) due to natural-abundance ^{57}Fe is indicated by *. A feature in (A) due to ^{14}N (see text) is indicated by #. Experimental conditions: (A) temperature, 2 K; microwave frequency, 34.60 GHz; microwave power, 1.2 mW; magnetic field, 1.190 T ($g = 2.08$); 100 kHz field modulation amplitude, 0.03 mT; time constant, 32 ms; rf scan rate, 1 MHz/s; rf power, 30 W; number of scans, 100; (B) same as in (A) except, microwave frequency, 34.63 GHz; magnetic field, 1.185 T ($g = 2.09$); 50 scans; (C) same as in (A) except, microwave frequency, 35.06 GHz; magnetic field, 1.204 T ($g = 2.08$); field modulation, 0.1 mT; 60 scans; (D) same as in (A) except, microwave frequency, 35.26 GHz; microwave power, 0.2 mW; magnetic field, 1.310 T ($g = 1.92$; this value was chosen so as to shift the proton pattern, labeled as ^{1}H, to the highest frequency); field modulation, 0.1 mT; 60 scans. A fourth-order polynomial baseline correction was used for spectra (A) and (D); none for the others. The relative spectral intensities are arbitrary.

Pf-Fd and an excess of either $K^{13}CN$ or $KC^{15}N$. In agreement with previous results,[34] no change in the EPR spectrum of this $S = {}^1/_2$ 3Fe-Fd was seen, and the ENDOR spectrum in the low-frequency region (taken at the single well-defined g value, $g = 2.01$, under experimental conditions similar to those used for the 4Fe-Fd) showed only a featureless baseline for both cyanide isotopologs. Thus, cyanide ion only interacts with the 4Fe-Fd.

Each of the ^{13}C and ^{15}N signals in Figure 3 is a hyperfine-split doublet centered at its respective Larmor frequency (when corrected for sweep-induced rf shifts: ≤0.2 MHz), as predicted by eq 1 ($\nu_C = 12.7$, $\nu_N = 5.1$ MHz; at 1.19 T); thus, at g_1, $A(^{13}C) \approx 2.5$ MHz and $A(^{15}N) \approx 1$ MHz. An additional signal at ~8 MHz seen in *Pf*-Fd-$C^{15}N$ (identified by # in Figure 3A) is assigned to the "double-quantum" transition of endogenous

(47) Houseman, A. L. P.; Oh, Byung-H.; Kennedy, M. C.; Fan, C.; Werst, M. M.; Beinert, H.; Markley, J. L.; Hoffman, B. M. *Biochemistry* **1992**, *31*, 2073–2080.
(48) Park, J.-B.; Fan, C.; Hoffman, B. M.; Adams, M. W. W. *J. Biol. Chem.* **1991**, *266*, 19351–19356.
(49) LaMar, G. N.; Adams, M. W. W., unpublished results.
(50) Doan, P. E.; Fan, C.; Hoffman, B. M. *J. Am. Chem. Soc.* **1994**, *116*, 1033–1041.

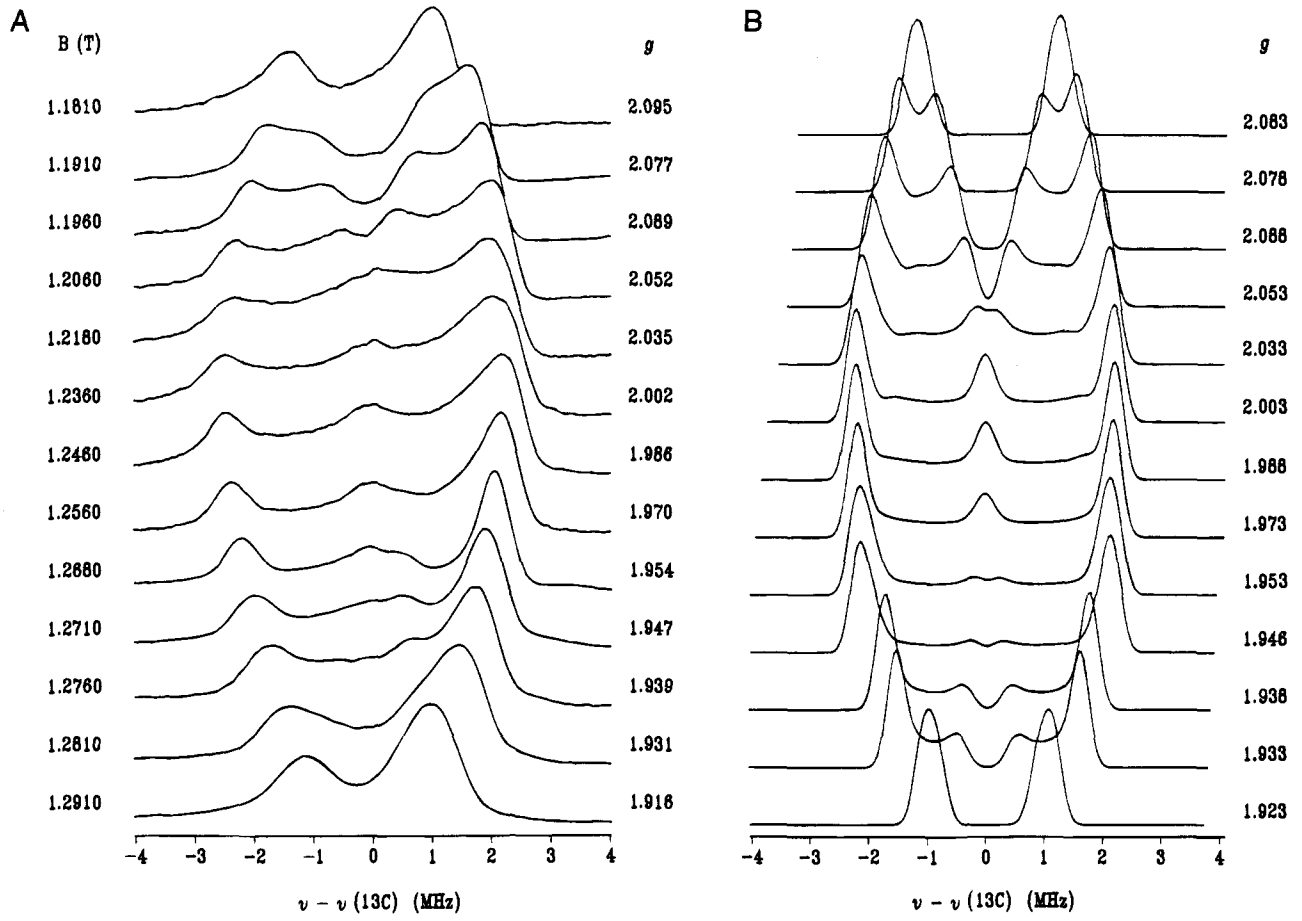

Figure 4. (A) ^{13}C ENDOR of *Pf*-Fd-^{13}CN. Each spectrum has been centered at its ^{13}C Larmor frequency ($\nu(^{13}C) \sim 13$ MHz). Experimental conditions are the same as in Figure 3B except for the magnetic field position as indicated. (B) Computer simulation of ^{13}C ENDOR signals for *Pf*-Fd-^{13}CN. The spectra are centered at $\nu(^{13}C)$ and are calculated at the g values indicated. Simulation parameters: $g = [2.09, 1.95, 1.92]$; $A(^{13}C) = [4.5, 4.5, -0.1$ MHz]; rotation of $A(^{13}C)$ about g_2 by $\Theta = 42°$; ENDOR line width (hwhm), 0.2 MHz; no EPR line width used.

^{14}N (e.g., peptide nitrogen), by analogy with 35 GHz ENDOR studies on other Fe-S proteins.[36,47] Although the *Pf*-Fd-$C^{15}N$ sample was at the same concentration as the *Pf*-Fd-^{13}CN (and natural abundance) samples, the ^{15}N ENDOR signal was much weaker than that seen for ^{13}C, making the adjacent ^{14}N "double-quantum" transition relatively more noticeable. We speculate that this relative difficulty in observing the ^{15}N ENDOR signal results from the virtual absence of isotropic coupling to the cluster (*vide infra*). Additional weak ^{14}N signals seen for *Pf*-Fd-CN at 3−4 MHz were not investigated further. As a final note, there is a very weak feature present in all samples at ~17 MHz, which we assign to natural-abundance ^{57}Fe (identified by * in Figure 3B). A complete study of ^{57}Fe-enriched *Pf*-Fd using Mössbauer and ENDOR spectroscopy is in progress.[51]

The ^{13}C ENDOR signal in Figure 3B is taken at the low-field edge of the EPR envelope. In this "single-crystal-like" field position,[36,52] only those molecules oriented so that the g_1 tensor axis is aligned with the field contribute to the observed ENDOR response. If the ^{13}C hyperfine coupling were isotropic, then as the magnetic field is increased (g decreased), the hyperfine splitting would remain unchanged and the doublet pattern would merely exhibit a linear shift to higher frequency due to the increase in ν_C. Instead, the spectra change dramatically as the field is increased, an indication of significant anisotropy in $A(^{13}C)$. This is shown in Figure 4A, where each spectrum has been centered at its ^{13}C Larmor frequency so as to emphasize spectral changes due to hyperfine anisotropy. As the field is increased from $g_1 = 2.09$, each partner of the hyperfine-split doublet seen at g_1 resolves itself into two, so that the full pattern is two doublets centered at ν_C. The splitting of the outer doublet increases with field until it reaches a maximum of $A(^{13}C) \sim 4.6$ MHz at $g = 1.98-1.99$, which is near to, but not coincident with, $g_2 = 1.95$. As the field is further increased, the splitting of this doublet then falls. The splitting of the inner doublet progressively decreases with increasing field until the two partner peaks coalesce at ν_C at $g \sim 2.0$; as the field is further raised, these peaks reappear as a doublet whose splitting increases with field (as that of the outer doublet decreases). Finally, as g_3 is approached, the two doublets merge and recombine into a single hyperfine-split doublet, as expected for this single-crystal-like position; the coupling at g_3 is $A(^{13}C) \approx 2.1$ MHz. As will be shown below, this field dependence can be described by that expected for a *single* nucleus whose hyperfine coupling tensor is dominated by anisotropic interactions. It is virtually impossible for two nuclei to exhibit identical anisotropic behavior, indicating that a single $^{13}CN^-$ binds to the cluster.

Following established procedures,[36-38] the full set of experimental peak positions can be matched quite well using the following parameters: $A_1(^{13}C) = -4.5(1)$, $A_2(^{13}C) = -4.5(1)$, $A_3(^{13}C) = +0.1(1)$ MHz, with $A(^{13}C)$ rotated about g_2 by $\Theta = 42(3)°$, where the uncertainties are given in parentheses. The relative signs are fixed by experiment; the absolute signs are arbitrarily chosen to make the largest anisotropic component positive.[53] Figures 4B and 5 present simulated spectra that use these parameters. The simulations in Figure 4B employ a

(51) Ravi, N.; Telser, J.; Smith, E. T.; Adams, M. W. W.; Hoffman, B. M.; Münck, E., manuscript in preparation.
(52) Rist, G. H.; Hyde, J. S. *J. Chem. Phys.* **1970**, *52*, 4633−4643.

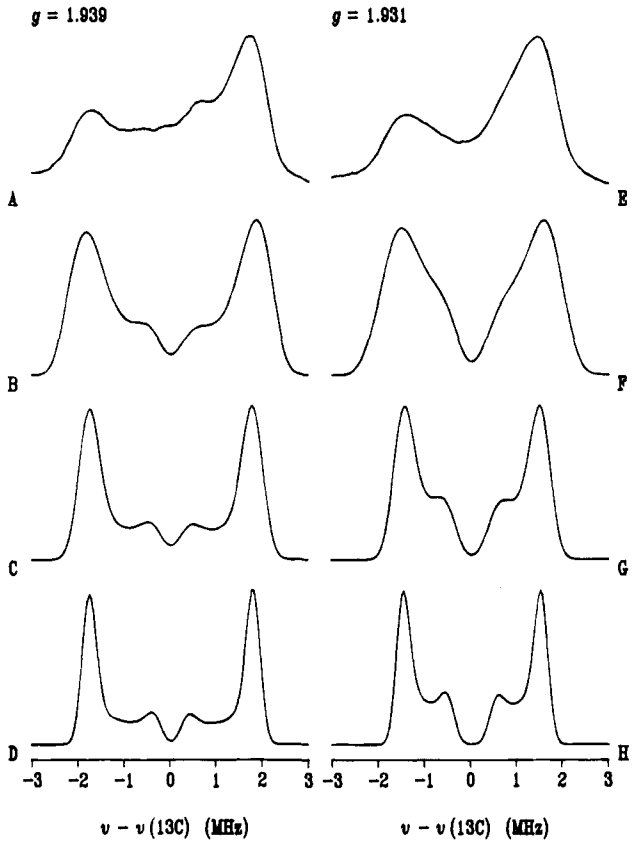

Figure 5. Comparison of experimental and simulated ^{13}C ENDOR spectra for *Pf*-Fd-^{13}CN showing the effects of ENDOR and EPR line widths on the simulated spectra. (A,E) Experimental spectra with conditions as in Figure 3B and (A) $\mathbf{B}_0 = 1.2760$ T ($g = 1.939$) and (E) $\mathbf{B}_0 = 1.2810$ T ($g = 1.931$). (B–D, F–H) Simulated spectra using the magnetic parameters given in Figure 4B and line widths as follows: (B,F) ENDOR, 0.3 MHz; EPR, 7 mT; (C,G) ENDOR, 0.3 MHz; EPR, 0 mT; (D,H) ENDOR, 0.2 MHz; EPR, 0 mT. The relative spectral intensities are arbitrary.

relatively narrow ENDOR line width (0.2 MHz hwhm) and do not include EPR line width effects. These are presented to allow a clear visualization of the field dependence of the ENDOR pattern as caused by the hyperfine anisotropy. As illustrated by Figure 5, a more realistic reproduction of the observed spectra requires both broader ENDOR lines and inclusion of EPR line width effects. This is particularly necessary to reproduce the spectral region between g_2 and g_3, where large changes in both the electronic and nuclear tensors occur within a narrow field range (<20 mT); these effects are much less significant in the spectral region between g_1 and g_2, because these two g values are well separated in field (by ~85 mT). To demonstrate the significance of these effects as well as the actual degree to which the experimental data is matched by the simulations, compare experimental spectra for $g = 1.931$ and 1.939, Figures 5A and 5E, respectively, to a series of simulated spectra using the above tensor parameters and with progressive line width increases. Figures 5D and 5H employ ENDOR line widths of 0.2 MHz and no EPR line widths (as in Figure 4B) and yield simulated spectra that are clearly too narrow. Figures 5C and 5G employ 0.3 MHz ENDOR line width; with this value the calculations match exactly the sharp features seen at g_2, and thus this width represents the "natural" ENDOR line width. However, with this ENDOR line width other sharp features are predicted, which does not match observation, while use of a larger ENDOR line width matches the signals observed in the complex spectral region between g_2 and g_3 at the expense of agreement with the sharp feature at g_2. To match theory and experiment it is necessary to include EPR line width effects in the simulations, which accounts for the fact that at a given field position (g value), the ENDOR signal arises from molecules whose EPR signal falls within a bandwidth of roughly $g \pm \delta g$, where δg is determined by the natural line widths of the single-crystal components of the powder-pattern EPR envelope; at 35 GHz and $g \approx 2$, $\delta g = 0.01$ corresponds to ~6 mT (180 MHz). This inclusion differentially broadens peaks that shift rapidly with field. As seen in Figures 5B and 5F, the experimental signals can indeed be reproduced quite well by the addition of an EPR line width of 7 mT (~0.011 in g).

Table 2. Hyperfine Coupling Constant Data (in MHz) for *Pf*-Fd-^{13}CN, Tf-^{13}CN, and Mb-^{13}CN and ^{15}N Hyperfine Coupling Constant Data for *Pf*-Fd-$C^{15}N$

		$A_1^{C/N}$	$A_2^{C/N}$	$A_3^{C/N}$	rotation angle
^{13}C	*Pf*-Fd-^{13}CN[a]	−4.5	−4.5	+0.1	$\Theta = 42°$
^{15}N	*Pf*-Fd-$C^{15}N$[b]	1.8	1.0	−2.4	−
		$T_1^{C/N}$	$T_2^{C/N}$	$T_{3dip}^{C/N}$	$a_{iso}^{C/N}$
^{13}C	*Pf*-Fd-^{13}CN	−1.5	−1.5	+2.9	−3.0
	Tf-^{13}CN[c]	4.47	−2.35	−2.12	−35.50
	Mb-^{13}CN[d]	−	−	−	28.64
^{15}N	*Pf*-Fd-$C^{15}N$	−1.7	−0.9	+2.5	−0.1

[a] For *Pf*-Fd-^{13}CN, uncertainties in the A values are ±0.1 MHz, and uncertainty in Θ is ± 3° (rotation of $\mathbf{A}(^{13}C)$ about g_2). Note that absolute signs are arbitrary. [b] For *Pf*-Fd-$C^{15}N$, uncertainties in the A values are ±0.3 MHz and no rotation of the $\mathbf{A}(^{13}C)$ from the $\mathbf{g}$ tensor could be determined. [c] Reference 55. For Tf-CN, we assign $g_1 = 2.34$, $g_2 = 2.15$, and $g_3 = 1.92$. The negative sign for a_{iso}^{C} was assigned by Snetsinger *et al.* for consistency with NMR data. [d] Reference 56. Note that the ^{13}C hyperfine coupling tensor was not determined.

Determination of the full $\mathbf{A}(^{13}C)$ tensor allows its principal components to be decomposed into isotropic (a_{iso}) and dipolar contributions: $A_i(^{13}C)_i = a_{iso} + T_i$ where $T_1 + T_2 + T_3 = 0$; these are summarized in Table 2. The isotropic coupling is small ($a_{iso} = -3.0$ MHz) and is comparable to the anisotropic contribution, whose largest component is $T_3 = +2.9$ MHz. Table 2 also includes ^{13}C hyperfine coupling for two monomeric metalloprotein low-spin Fe^{3+}–^{13}CN systems: cyanotransferrin (Tf-^{13}CN),[55] and cyanometmyoglobin (Mb-^{13}CN).[56] Note that with Mb-^{13}CN only $A_z(^{13}C)$ was reported, although the coupling was thought to be largely isotropic.[56] The mononuclear centers in these reference metalloproteins as well as other transition metal cyano complexes (e.g., $Cr(^{13}CN)_6^{3-}$ [57] and $Fe(^{13}CN)_6^{3-}$ [58,59]) each have a large (negative) isotropic ^{13}C hyperfine coupling constant, $a_{iso}^{C} \approx -30$ MHz (NMR studies showed that the absolute sign is negative[58]). This coupling has been ascribed to exchange polarization between the unpaired electron in the metal d orbital and cyanide σ-bonding paired electrons.[57] The small corresponding value for *Pf*-Fd-^{13}CN, $a_{iso}(^{13}C) = -3$ MHz, shows there to be very little spin delocalization or exchange polarization into the σ-bonding system of the cyanide ligand; the absence of higher frequency ^{13}C signals (Figure 3D)

(53) In the case of the mononuclear Fe of Tf-^{13}CN,[55] $T > 0$; for the spin-coupled cluster of *Pf*-Fd-^{13}CN, either choice of overall signs for A and thus either sign of T is possible, depending on whether the spin-coupling coefficient of the Fe is positive, as would be the case of the oxidized $Fe^{2.5+}$ sites of a $[4Fe\text{-}4S]^{+}$ cluster, or negative, as with the reduced (Fe^{2+}) sites.[54]

(54) Mouesca, J.-M.; Chen, J. L.; Noodleman, L.; Bashford, D.; Case, D. A. *J. Am. Chem. Soc.* **1994**, *116*, 11898–11914.

(55) Snetsinger, P. A.; Chasteen, N. D.; van Willigen, H. *J. Am. Chem. Soc.* **1990**, *112*, 8155–8160.

(56) Mulks, C. F.; Scholes, C. P.; Dickinson, L. C.; Lapidot, A. *J. Am. Chem. Soc.* **1979**, *101*, 1645–1654.

(57) Kuska, H. A.; Rogers, M. T. *J. Chem. Phys.* **1964**, *41*, 3802–3805.

(58) Lowenstein, A.; Shporer, M.; Navon, G. *J. Am. Chem. Soc.* **1963**, *85*, 2855–2856.

(59) Davis, D. G.; Kurland, R. J. *J. Chem. Phys.* **1967**, *46*, 388–390.

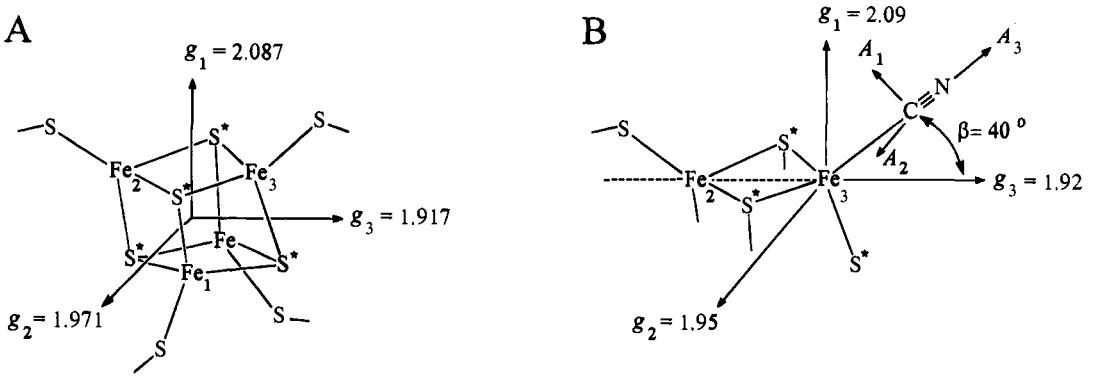

Figure 6. Idealized representation of the $[Fe_4S_4]^+$ cluster in (A) the model compound, $[Fe_4S_4(SCH_2Ph)_4]^{3-}$, and (B) *Pf*-Fd-CN. Inorganic sulfide ions are indicated by asterisks and iron ions are identified by the numbering scheme of Gloux *et al.*[63] The approximate orientation of the **g** tensor with respect to the molecular framework for center II_R determined by these workers[63] is shown in (A). The proposed orientation of the **g** tensor, the **A**(^{13}C) tensor, and the bound cyanide ligand in *Pf*-Fd-CN is shown in (B). For clarity, in (B) the lower portion of the cluster is not shown and the **g** tensor has been translated from the cube center to the unique (cyanide-bound) Fe to emphasize the relative orientations of the **g** and **A**(^{13}C) tensors. The rotation angle, $\beta \approx 40°$, of A_3(^{13}C) from g_3 is also indicated.

confirms there is no other, more strongly bound, CN^-. Both *Pf*-Fd-^{13}CN and Tf-^{13}CN have weak anisotropic ^{13}C hyperfine interactions with coupling tensors (**T**(^{13}C)) that have the classical dipole form, with tensor elements $(2T, -T, -T)$, where $T \approx$ 1.5 and 2.2 MHz, respectively.[53] The similarity of the through-space dipolar couplings highlights the dramatically different through-bond components.

The ^{15}N ENDOR data obtained for *Pf*-Fd-C^{15}N provide further support for the above analysis. Spectra recorded at magnetic fields across the EPR envelope (data not shown) again show paired features centered at the appropriate ^{15}N Larmor frequency, with small hyperfine coupling: $A(^{15}N) < 2.2$ MHz. In the case of ^{15}N, the hyperfine coupling near g_2 is a minimum rather than a maximum as with ^{13}C. Despite the lower quality of these spectra, it was possible to estimate the ^{15}N hyperfine tensor components (Table 2), leading to a tensor with virtually no isotropic component. However, it was not possible to determine accurately the orientation of the **A**(^{15}N) with respect to the **g** tensor as was done above for ^{13}C. For comparison, a single-crystal EPR/ENDOR study by Wang and de Boer, on $Fe(CN)_6^{3-}$ doped into KCl, reported the full ^{14}N hyperfine and quadrupole tensors and found that the ^{14}N and ^{13}C hyperfine tensors were exactly collinear.[60] We assume this here as well.

In the case of *Pf*-Fd-C^{15}N there is virtually no isotropic hyperfine coupling to ^{15}N (which is not directly bound to Fe), $a_{iso}(^{15}N) \approx -0.1$ MHz, consistent with the small coupling to ^{13}C (that is bound to Fe). For $Fe(CN)_6^{3-}$ it was found that $a_{iso}(^{14}N) = 0.36$ MHz;[60] from the ratio $g_N(^{15}N)/g_N(^{14}N) = 1.403$ this corresponds to an isotropic coupling of $a_{iso}(^{15}N) = 0.51$ MHz. Thus, even with typical isotropic ^{13}C couplings of ~30 MHz (as also found in that study), the corresponding nitrogen coupling is quite small, although still significantly larger than that observed for *Pf*-Fd-C^{15}N ($a_{iso}(^{14}N) \leq 0.1$ MHz).

Geometrical Model for Cyanide Binding. Despite the lack of crystallographic data for *Pf*-Fd, it is possible to propose a simple geometrical model for cyanide bonding to the $[Fe_4S_4]^+$ cluster. To do this, we first relate the **g** tensor orientation to the cluster geometry by making use of the beautiful single-crystal EPR/ENDOR studies by Gloux, Lamotte, and co-workers.[61-65] These workers prepared γ-irradiated crystals of the 4Fe-Fd model compounds $(Et_4N)_2[Fe_4S_4(SR_4)]$, where R = Ph[61,66] and CH_2Ph,[62-64] synthesized with natural-abundance Fe[61,63,66] and ^{57}Fe.[64] Irradiation of the $[Fe_4S_4]^{2+}$ starting material generated a number of magnetically distinct sites for both the oxidized cluster core, $[Fe_4S_4]^{3+}$, and the reduced core, $[Fe_4S_4]^+$. For comparison with the $[Fe_4S_4]^+$ cluster of *Pf*-Fd-CN, we have selected the reduced center II_R of ref 63 (which is similar to center A of $[Fe_4S_4(SPh_4)]$;[66] see Table 1) rather than the other reduced center (I_R of ref 63), because the **g** tensor of center II_R corresponds quite closely to that of *Pf*-Fd-CN while center I_R does not (see Table 1).

Gloux *et al.* have definitively determined the **g** tensor for this reduced, $[Fe_4S_4(SCH_2Ph)_4]^{3-}$, species (center II_R) to have an orientation as indicated in Figure 6A: $g_1(max) = 2.087$ is along the cluster (approximate) S_4 axis (i.e., normal to the Fe-Fe diagonals that bisect the cube faces, offset from Fe_1-Fe_4 ⊗ Fe_2-Fe_3 by 6°); $g_2(mid) = 1.971$ lies along the Fe_1-Fe_4 vector (actually offset by 16°); and $g_3(min) = 1.917$ lies along the Fe_2-Fe_3 vector (actually offset by 17°).[63] These workers have also determined that the Fe ions have the same oxidation state in pairs, as follows: if $Fe_{1,4}$ are the ferrous pair, then $Fe_{2,3}$ is the mixed-oxidation state pair or *vice versa*. In the oxidized, $[Fe_4S_4(SCH_2Ph)_4]^-$, species (center IV; studied by ENDOR[64]), the **g** tensor orientation and oxidation state assignments are quite similar, and the assignment of Fe oxidation states to specific Fe ions has been made.[67] No assignment has yet been made as to the oxidation states of the individual Fe ions in site II_R of the reduced, $[Fe_4S_4]^+$, model compound.[63]

By analogy with these general results for reduced (and oxidized) cluster model compounds, for *Pf*-Fd-CN we can assign $g_1(max) = 2.09$ to lie along the cluster S_4 axis and the other two directions, $g_2(mid) = 1.95$ and $g_3(min) = 1.92$, to coincide with Fe-Fe vector with each pair of Fe ions so connected having the same oxidation state. This orientation is shown for *Pf*-Fd-CN in an idealized form in Figure 6B. In order to focus on the cyanide-bound Fe and its immediate environment, we have removed the lower portion of the cluster and translated

(60) Wang, D. M.; de Boer, E. *J. Chem. Phys.* **1990**, *92*, 4698-4707.
(61) Gloux, J.; Gloux, P.; Lamotte, B.; Rius, G. *Phys. Rev. Lett.* **1985**, *54*, 599-602.
(62) Mouesca, J.-M.; Rius, G.; Lamotte, B. *J. Am. Chem. Soc.* **1993**, *115*, 4714-4731.
(63) Gloux, J.; Gloux, P.; Lamotte, B.; Mouesca, M.-M.; Rius, G. *J. Am. Chem. Soc.* **1994**, *116*, 1953-1961.
(64) Rius, G.; Lamotte, B. *J. Am. Chem. Soc.* **1989**, *111*, 2464-2469.
(65) Mouesca, J.-M., personal communication and unpublished work cited in ref 63.
(66) Gloux, J.; Gloux, P.; Hendriks, H.; Rius, G. *J. Am. Chem. Soc.* **1987**, *109*, 3220-3224.
(67) The definitive **g** tensor orientation and oxidation state assignment in center IV is as follows: $g_1(max) = 2.070$ is along the S_4 axis (actually offset by 16°), $g_2(mid) = 2.026$ lies along the Fe_1^{3+}-Fe_2^{3+} vector (actually offset by 17°), and $g_3(min) = 2.018$ lies along the $Fe_3^{2.5+}$-$Fe_4^{2.5+}$ vector (actually offset by 6°). Note that these g values were previously reported as 2.066, 2.025, and 2.014.[64]

the g tensor coordinate system to an origin at this Fe. As noted immediately above, this Fe could be of either type.[53]

The next step is to use ENDOR data to relate the ^{13}C hyperfine tensor to the molecular system. To accomplish this we again make use of the single-crystal study of $Fe(CN)_6^{3-}$ by Wang and de Boer.[60] They found that in $Fe(CN)_6^{3-}$ the ^{14}N (and ^{13}C) hyperfine tensor directions corresponded to Fe−CN bond vectors.[60] One principal value of their rhombic ^{14}N tensor ($A_3(^{14}N)$, that along the molecular z axis) was aligned exactly with the Fe−CN bond vector and the other two (A_1 and $A_2(^{14}N)$, those in the molecular x,y plane) were each rotated by only ~8° from the appropriate Fe−CN vector. Their results suggest that the orientation of the hyperfine tensors is largely determined by the local bonding geometry, so that one of the principal directions of $A(^{13}C)$ must correspond to the Fe−CN σ-bond vector. We thus assign the direction of the unique hyperfine component, $A_3(^{13}C)$, as corresponding to the Fe−CN bond vector (see Figure 6B). The ^{13}C ENDOR simulations showed that the $A(^{13}C)$ tensor is rotated $\beta = 42 \pm 3°$ about g_2 (i.e., in the plane defined by g_1 and g_3). Thus the g_2 and $A_2(^{13}C)$ axes are collinear while $A_1(^{13}C)$ and $A_3(^{13}C)$ lie between (roughly bisecting) the g_1 and g_3 axes. Since the direction of g_2 corresponds to an Fe−Fe vector (1,4 or 2,3), so then does the direction of $A_2(^{13}C)$ while $A_3(^{13}C)$, and thus the Fe−CN bond, lies ~40° from the other Fe−Fe vector (defined by g_3).

The resulting assignment of the orientations of the $A(^{13}C)$ and g tensors in *Pf*-Fd-CN shown in Figure 6B is consistent with a simple replacement by cyanide ion of one alkyl thiolate from an ordinary tetrathiolate coordinate [4Fe-4S] cube. This can be easily demonstrated using the structural data on the $[Fe_4S_4(SCH_2Ph)_4]^{2-}$ model cluster, crystallographically characterized by Averill *et al.*[68] Defining the angles β' as those between the two Fe−Fe vectors that correspond to g tensor directions and the Fe−S(R) bonds, there are four such angles in $[Fe_4S_4(SCH_2Ph)_4]^{2-}$, one for each Fe−SR unit.[68] We determine these to be as follows: $\beta'(Fe_4-Fe_1-S_5)$, 33.7°; $\beta'(Fe_1-Fe_4-S_8)$, 31.4°; $\beta'(Fe_3-Fe_2-S_6)$, 37.9°; $\beta'(Fe_2-Fe_3-S_7)$, 37.2°. Averaging the two types of Fe ion gives $\beta' = 32.5°$ for $Fe_{1,4}$ and 37.5° for $Fe_{2,3}$. Thus the structural data for the model cluster give an average rotation angle of the thiolate ligand from the Fe−Fe vector of $\beta' = 35 \pm 5°$, in reasonable agreement with the ENDOR-based assignment of the Fe−C≡N vector for *Pf*-Fd-CN ($\beta = 42 \pm 3°$). If the EPR-based assignment (*vide supra*) of the g_3 direction to the Fe_2-Fe_3 direction is incorporated,[63] then only the $Fe_{2,3}$ value ($\beta' = 37.5°$) is relevant. Thus the ENDOR data and analysis lead to an extremely satisfying geometric picture, which strongly suggests that CN^- replaces the Asp-14 ligand rather than binding to give a 5-coordinate Fe.

(68) Averill, B. A.; Herskovitz, T.; Holm, R. H.; Ibers, J. A. *J. Am. Chem. Soc.* **1973**, *95*, 3523−3533.
(69) Noodleman, L. *Inorg. Chem.* **1991**, *30*, 246−256.

Conclusions

Pf-Fd contains an $[Fe_4S_4]^+$ cluster that is unusual for two reasons. It exists as a mixture of spin states, $S = {}^1/_2$ and $S = {}^3/_2$. More interestingly, it is ligated by only three Cys residues with two viable candidates for the remaining ligand: water/hydroxide from solvent or asparate, the residue replacing the Cys normally found at that position in 4Fe-Fd's. An earlier study from this laboratory favored the water/hydroxide, based on the observation of a strongly coupled solvent-exchangeable ^1H ENDOR signal ($A^H = 22$ MHz).[48] However, the present study does not confirm that suggestion, and NMR measurements support the assignment to Asp.[49]

The addition of excess cyanide ion converts the cluster exclusively to the $S = {}^1/_2$ state, but one electronically distinct from the native $S = {}^1/_2$ species, because the g values are markedly different. ENDOR using natural-abundance cyanide and the isotopologs, $^{13}CN^-$ and $C^{15}N^-$, shows the presence of a single bound cyanide ion. Its properties, however, are quite different from those seen for cyanide binding to monomeric low-spin Fe(III) proteins such as transferrin and myoglobin, as well as in analogous small molecules. In these instances there is a large isotropic ^{13}C hyperfine coupling constant (~−30 MHz), indicating significant spin delocalization onto the cyanide ligand. In contrast, for *Pf*-Fd-CN, the isotropic coupling is negligible (~−3 MHz for ^{13}C), although the strong effect on cluster electronic structure indicates direct binding. Using the analytical technique of orientation-selective ENDOR,[36−38,43,44] the cyanide ligand has been used as a spectroscopic probe of the *Pf*-Fd-CN cluster geometry. By combining the ENDOR data with single-crystal structural and EPR/ENDOR data on $[Fe_4S_4]^{+,3+}$ model compounds and on $Fe(CN)_6^{3-}$, we find that the cyanide ligand binds analogously to and has the same orientation as the Cys ligand commonly found in 4Fe-Fd's, and thus appears to replace Asp-14. To extrapolate from this finding, it suggests that ligand exchange can occur in $[Fe_4S_4]$ clusters without perturbing the cluster itself. Such behavior is essential for long-lived catalytic activity.

Acknowledgment. This work was supported by grants from the NSF (DMB-8907559 to B.M.H., a Research Opportunity Award to J.T., Research Training Group Award DIR-9014281 to the Center for Metalloenzyme Studies, and instrumentation grant DIR-9102055 to M.K.J.) and the NIH (GM-45597 to M.W.W.A. and M.K.J.). We thank Dr. Peter E. Doan for helpful discussions on ENDOR simulations and Dr. David M. Eichhorn for assistance with the crystallographic analysis.

JA943577N